Processing gravity gradients to detect kimberlite pipes

Tom Meyer *
Lockheed Martin MST, New Ventures – Gravity Systems
Niagara Falls, NY (USA)
Tom.J.Meyer@LMCO.com

SUMMARY

A modelling and pattern recognition-based approach is applied to processing airborne gravity gradient data for kimberlite exploration. The carrot-like bodies with low density crater facies that typify kimberlite pipes are particularly amenable to this treatment.

Results for small and medium-sized pipes buried deeply beneath nominal geologic clutter are promising. Details regarding various error rates provide valuable input to exploration programs and the framework can include any data type.

A three-class problem is formulated to address the case of false alarms. A first example is worked for low density shallow depressions that closely mimic gravity images of pipes, providing insight to what is needed from a survey fidelity standpoint to effectively mitigate false alarms.

Key words: gravity, gradiometry, kimberlite, detect

INTRODUCTION

Exploring for kimberlite with various remote sensing methods typically calls for high resolution imaging owing to the small scale of pipes and their signatures. Airborne gravity gradiometry can deliver this capability (Barnes, 2011) and sees growing consideration in programs. Among its benefits include: i.) aircraft motion being common-mode rejected thus the GPS-limit does not apply and short wavelength gravity signals are acquired, ii.) geo-registration errors having only a second-order influence on measured gradients versus a first-order influence for gravity surveys, and iii.) high coverage rates without ground accessibility problems.

With gradiometry survey in-hand the interpreter scrutinizes data at a fine scale to identify and accredit each anomaly with an underlying kimberlite pipe or not, then ascertains confidence levels for each decision. One thus hopes to make a binary decision, though ambiguities and weak signals are often assigned a less desirable third outcome that may be loosely described as "too difficult to decide."

PATTERN RECOGNITION FRAMEWORK

Discriminant analysis can aid the interpretation process. Linear projections applied here aim to attenuate gradient data content lying in the unwanted clutter subspace (signal induced by terrain and nominal subsurface geologic variations, plus instrument noise) while amplifying content lying in the target subspace (signal induced by kimberlite pipes). The overlap of these two subspaces directly relates to the difficulty of the detection problem. At one extreme if the two subspaces do not intersect the detection is trivial; at the other extreme if the subspaces are wholly coincident the detection problem may be impossible. Using gravity gradients to detect pipes is between these two extremes making acceptable detection challenging, but workable.

A No Kimberlite (NK) *class* is defined and typified by the data ensemble X_{NK} comprising boxcar-windowed sections of gravity gradient data x_{dens} collected above nominal terrain and geologic variations (Figure 1), plus added noise x_{instr} owing to the gradiometer instrument

$$X_{NK} = \left\{ x_{NK,j} : \quad x_{NK,j} = x_{dens,j} + x_{instr,j} \right\}$$

Each data window of X_{NK} is a *member* of class NK. Ideally, the ensemble is very large with every anticipated terrain, geologic setting, and instrument noise represented. Similarly, a Kimberlite Pipe (KP) class is defined and typified by the data ensemble X_{KP} comprising data from windowed sections placed above pipes causing gradient anomalies x_{pipe} superposed on terrain and geology-induced background gradients, plus instrument noise

$$X_{KP} = \left\{ x_{KP,k} : \quad x_{KP,k} = x_{dens,k} + x_{instr,k} + x_{pipe,k} \right\}$$

A scalar *feature* is extracted from each member by projecting associated data along a common unit direction a. This is implemented via dot product operator $y = a \cdot x$, which condenses each member's original data dimension to a scalar value. Each of the two classes is subsequently defined also by their ensembles of these scalars or feature *populations*

$$Y_{NK} = \left\{ y_{NK,j} : \quad y_{NK,j} = a \cdot x_{NK,j} \right\}$$
$$Y_{KP} = \left\{ y_{KP,k} : \quad y_{KP,k} = a \cdot x_{KP,k} \right\}$$

The notion of extracting scalar features from data is not unlike "bump finding" when visually examining data. Here, however, a judiciously chosen projection a can amplify differences between the two classes helping to make one population distinct from the other when overlaid as histograms on a real number axis (Figure 2). A simple threshold detector is effective if the two classes are significantly distinct from one another as the figure suggests.
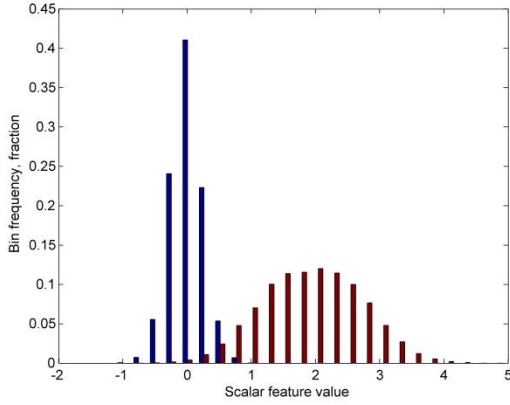
Figure 2: Overlaid histograms of significantly distinct classes. Feature values greater than a threshold of 0.5 belong primarily to the class shown with lighter shading.

Classes are distinct if their populations have small *intra-class spread* but large *inter-class separation*. An effective way to minimize intra-class spread while maximizing inter-class separation is to solve for a unit direction a giving the maximum separation-to-spread ratio (S_b/S_w) defined by

$$J^* = \max_a \left(\frac{S_b}{S_w} \right) = \max_a \left(\frac{a^T (\bar{x}_{KP} - \bar{x}_{NK})(\bar{x}_{KP} - \bar{x}_{NK})^T a}{a^T (\Sigma_{KP} + \Sigma_{NK})a} \right)$$

The numerator aligns a with the difference between class means giving an image similar to that of kimberlite pipes, but the denominator avoids aligning a with strong noise, which is evident on writing the population variances as a sum of noise components with strengths λ_j and unit directions v_j

$$a^T (\Sigma_{KP} + \Sigma_{NK})a = a^T V \Lambda V^T a = \sum_j \left(\lambda_j^{1/2} a \cdot v_j \right)^2$$

Shallow depressions filled with low density sediment are strong noise components that can closely mimic the gravity image of a kimberlite pipe. For such cases the projection aligns with more subtle class differences, which may be too subtle to note by visual inspection, and requiring state-of-the-art gradiometer fidelity for registering. The solution to J^* is

$$a = n / \|n\| \quad , \quad n = (\Sigma_{NK} + \Sigma_{KP})^{-1} (\bar{x}_{KP} - \bar{x}_{NK})$$

EXAMPLE KIMBERLITE PIPE DETECTION

The preceding discussion assumes large data ensembles that are *labelled,* wherein for each data window the presence or absence of pipes is known and data is assigned to the proper class and a projection is found. Labelled ensembles are generated in lieu of actual field data.

Voxets with fractal density distributions are used to forward model a large number of mock surveys. The vertical gradient *Gzz* is used exclusively throughout this study. All gradiometry surveyors can derive this data product from their particular gradiometer systems. The vertical gradient also seems somewhat favoured in literature perhaps owing to its maintaining spatial coincidence with underlying features (similar to how reduction to pole is favoured for viewing mag data). The scale of *Gzz* anomalies is commensurate with field data reported elsewhere (e.g. Hatch, 2004). Spectral character

of gradients varies on a per survey basis through the fractal density generator giving coarse to fine *Gzz textures* (for reference, the data image of Figure 1 exhibits moderate *Gzz* texture).

Pipes are modelled as inverted cones similar to (Allen, 2001) and then divided into crater, diatreme, and hypabyssal facies depth zones. Density anomalies are assigned to each zone relative to a homogeneous reference value (Table 1), guided by values reported in (Power, 2007). Focus here is on moderate and small pipes of roughly 6 and 2 hectare, respectively, with burial depths ranging from just a few meters to 100 m.

Feature	Density anomaly, g/cm³
Fractal background geology variations	−0.15 to +0.15
Crater facies	−0.30 to −0.10
Diatreme facies	Gradated to join adjacent zones
Hypabyssal facies	−0.10 to +0.15

**Table 1: Ranges of density anomalies of various modelled features.**

The synthetic data ensembles are processed in a *training phase* to determine an optimum projection a as outlined above, which is then used to extract the scalar feature populations from both classes giving overlaid histograms similar to Figure 2. A threshold is swept along the real axis while tallying classification errors at each value. Detection and false alarm rates are plotted for each threshold value as a receiver operating characteristic (ROC) curve (Figure 3). Having decided an acceptable false alarm rate (i.e., how often one thinks a pipe exists at a particular location when in fact it does not) the ROC curve quickly conveys the associated detection success rate.

Before applying the projection to actual field data to help discover pipes, it is tested against independent data ensembles in a *testing phase*. This phase applies the projection already in-hand to previously unseen geologic settings and pipes while tallying errors for each threshold value. These ROC curves are then overlaid with the ones obtained during training to verify performance stability (Figure 3). Projections can also be used to filter survey data (Figure 4). Equally important to clearly showing pipe presence, the filtered data does not suggest pipes for the many visually pipe-like anomalies in the unfiltered survey data.

THE THREE CLASS PROBLEM

As a first-cut at constructing and training against an ensemble of structured non-pipe features that cause gradient anomalies mimicking those of pipes, a False Target (FT) class is added comprising shallow depressions filled with low density sediment. Class FT is defined and typified by the data ensemble X_{FT} comprising boxcar-windowed sections of gravity gradient data x_{dens} collected above nominal terrain and geologic variations, plus added noise x_{instr} owing to the gradiometer instrument and the signal induced by the shallow depression filled with low density sediment, $x_{shal\,depress}$

$$X_{FT} = \left\{ x_{FT,m} : \quad x_{FT,m} = x_{dens,m} + x_{instr,m} + x_{shal\,depress,m} \right\}$$
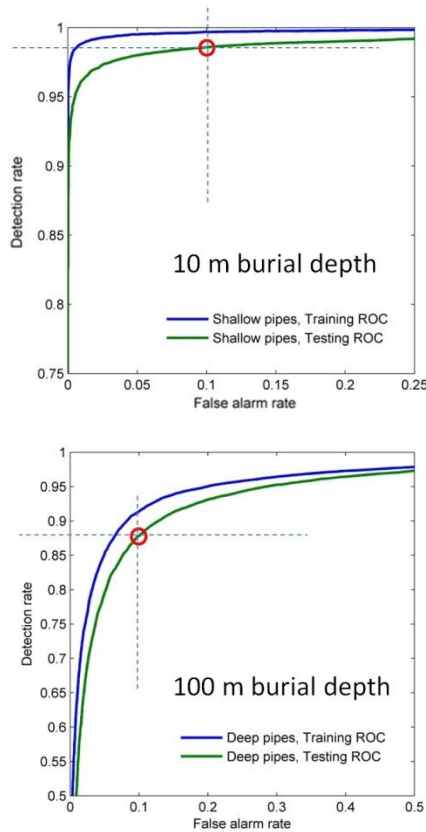
Figure 3: ROC curves for shallow and deep burials of small and medium pipes from the training (blue traces) and testing phases (green traces) of the classifier design show good agreement.

Two projections are found for this three-class problem by maximizing a generalized separation-to-spread ratio similar to that previously shown for the two-class scenario. The feature space is now two-dimensional, i.e., two features are extracted, one per projection, versus a single scalar being extracted from each class member. The notions of intra-class spread and inter-class separation also carry over.

The signals $x_{shal\ depress}$ for each member of class FT comprise the forward-modeled Gzz gradient owing to an instance of a deformable template of a shallow depression (Table 2).

Attribute	Range
Diameter at top of depression	150 to 400 m
Depth	20 to 100 m
Depth of burial	0 to 20 m
Skew (horizontal offset of bottom as fraction of total depth)	0 to 0.5
Density contrast	-0.17 g/cm^3
Edge profile	Varied

Table 2: Characteristics of modelled shallow depressions.

Sharing a very similar shape and scale, the anomalous gradient signals induced by the shallow depressions are very difficult to visually distinguish from those induced by kimberlite pipes. However, if the gradiometry instrumentation and survey fidelity are sufficient to register these differences, then by following the framework outlined above two projections are

found that isolate and amplify these subtle differences in an attempt to make the features extracted from the three classes mutually distinct.

Figures 5 and 6 show the resulting feature populations for shallow and deep burial of small and medium pipes obtained during the training and testing phases. Decision curves are sketched to show the possible trade of false alarm rate for increased detection rate. The curves are drawn the same for both phases, showing robustness of the feature extractions. The blue decision curve favours higher detection rate at the expense of absorbing more false alarms. The red decision curve favours fewer false alarms at the opportunity cost of missing some buried pipes.
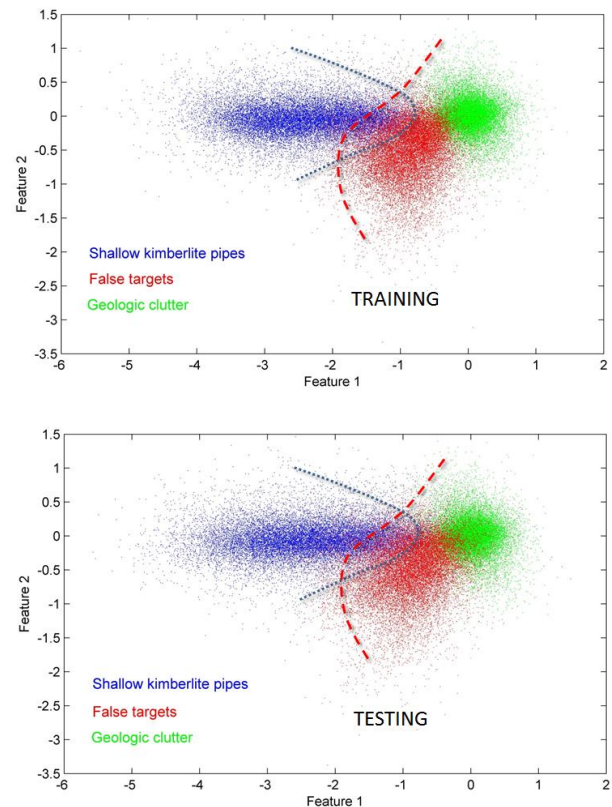
Figure 5: Feature populations for the three-class problem with shallow burial of small and medium-sized pipes.

As one would expect, classes are less distinct for the deep burial scenario than for shallow burials. However, the sketched decision curve suggests the majority of small and medium pipes would be found with some moderate false alarm rate incurred.

CONCLUSIONS

Preliminary results of new gravity gradient processing methods suggest 98% of shallow pipes and 88% of deeply buried pipes might be discovered with only 1 in 10 false alarms incurred if pipes exist in nominally unstructured geologic settings, i.e., free of specific structured anomalies whose gradient signals closely mimic those of pipes. The development is extended to a three-class problem by constructing and training against an ensemble of shallow depressions that cause gradient anomalies mimicking those of pipes. Results clearly show how measurement fidelity relates

to class distinction and subsequent detection success. Adding more geologic expertise and actual field data will enhance the overall approach to the point one could confidently reduce this approach to practice. Other extensions include adding context dependent classification, since pipes tend to occur in clusters. A large return is expected by processing multiple data types within this framework, including context dependency to acknowledge physical relations between observables, e.g., correlations between resistivity lows and density lows.

REFERENCES

Allen, T. et al., 2001. High definition gravity surveys and density modelling for kimberlite exploration. Exploration Geophysics: 32, 089-094.

Barnes, G. and Lumley, J. 2011. Processing gravity gradient data. Geophysics: Vol. 76, No. 2, 133-147.

Hatch, D. 2004. Evaluation of a full tensor gravity gradiometer for kimberlite exploration. Airborne Gravity 2004: Abstracts from the ASEG-PESA Airborne Gravity 2004 Workshop, 73-79.

Power, M. and Hildes, D. 2007. Geophysical strategies for kimberlite exploration in northern Canada. Proceedings of Exploration 07: Fifth Decennial International Conference on Mineral Exploration, 1025-1031.
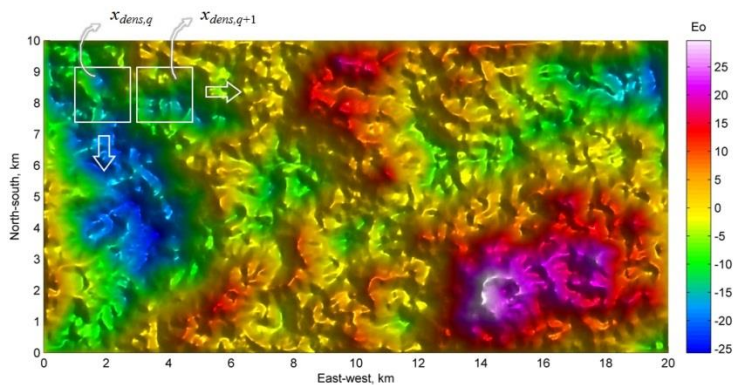
Figure 1: Example scene void of pipes. A window is placed at multiple locations to retrieve exemplars of vertical gravity gradient data induced by background geology and residual terrain effects.
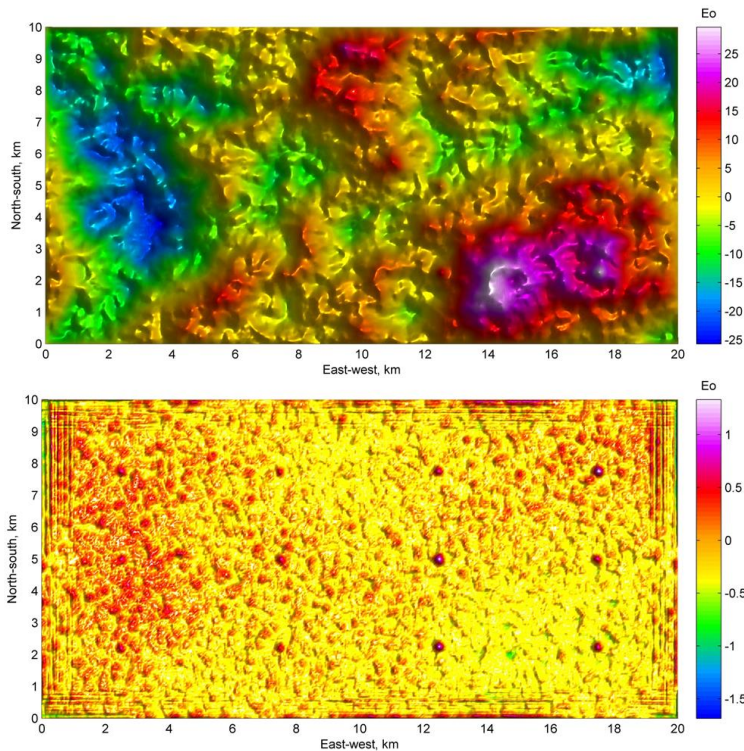
Figure 4: A survey image with many ambiguities (top) and its filtered image revealing six small and six medium pipes regularly placed to the left and right halves of the image, respectively.
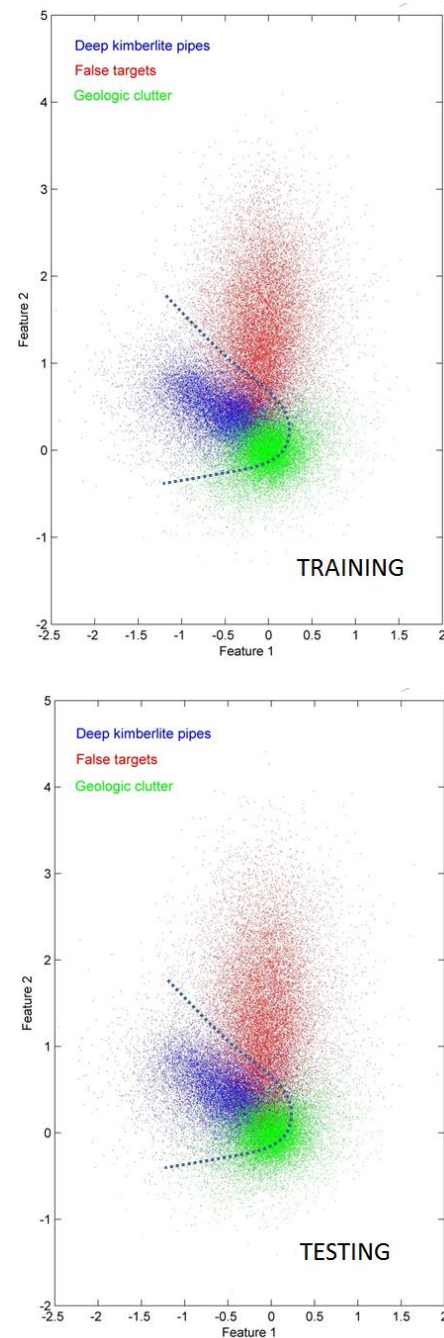
Figure 6: Feature populations for the three-class problem with deep burial of small and medium-sized pipes.